




Evidence for current-induced phase coexistence in  $\text{Ca}_2\text{RuO}_4$  and its influence on magnetic orderK. Jenni,<sup>1</sup> F. Wirth,<sup>1</sup> K. Dietrich,<sup>1</sup> L. Berger,<sup>1</sup> Y. Sidis,<sup>2</sup> S. Kunkemöller,<sup>1</sup> C. P. Grams <sup>1</sup>,  
D. I. Khomskii,<sup>1</sup> J. Hemberger <sup>1</sup> and M. Braden <sup>1,\*</sup><sup>1</sup>*II. Physikalisches Institut, Universität zu Köln, Zùlpicher Strasse 77, D-50937 Köln, Germany*<sup>2</sup>*Laboratoire Léon Brillouin, C.E.A./C.N.R.S., F-91191 Gif-sur-Yvette CEDEX, France*

(Received 4 May 2020; revised 29 June 2020; accepted 13 July 2020; published 3 August 2020)

Combining quasistatic and time-resolved transport measurements with x-ray and neutron diffraction experiments we study the nonequilibrium states that arise in pure and in Ti-substituted  $\text{Ca}_2\text{RuO}_4$  under the application of current densities. Time-resolved studies of the current-induced switching find a slow conductance relaxation that can be identified with heating and a fast one that unambiguously proves an intrinsic mechanism. The current-induced phase transition leads to complex diffraction patterns. Separated Bragg reflections that can be associated with the metallic and insulating phases by their lattice parameters, indicate a real structure with phase coexistence that strongly varies with temperature and current strength. A third contribution with a  $c$  lattice constant in between those of metallic and insulating phases appears upon cooling. At low current densities, this additional phase appears below  $\sim 100$  K and is accompanied by a suppression of the antiferromagnetic order that otherwise can coexist with current carrying states. A possible origin of the intermediate phase is discussed.

DOI: [10.1103/PhysRevMaterials.4.085001](https://doi.org/10.1103/PhysRevMaterials.4.085001)

## I. INTRODUCTION

The interaction of magnetic, orbital, and lattice degrees of freedom in strongly correlated electron materials frequently leads to the competition of different phases. As a result, small external stimuli can trigger phase transitions and exotic quantum states. Specifically, the electric control of nonthermal phase transitions is of wide interest in view of possible applications [1,2]. It is, however, very difficult to establish a true nonequilibrium character of a new phase and to fully exclude Joule heating or microscopic phase separation, which were shown to be relevant in many  $3d$  transition-metal oxides [3,4]. For electric-field-induced phenomena it was shown that the motion of defects can be essential [5,6]. Therefore, a thorough understanding of the transition mechanisms is essential for the interpretation of any nonequilibrium phase.

In this paper, we investigate the antiferromagnetic (AFM) Mott insulator  $\text{Ca}_2\text{RuO}_4$ , which is a “bad metal” (with low conductance) at high temperatures in thermal equilibrium and which transforms into a Mott insulator upon cooling below 357 K [7–9]. The metal-insulator transition is accompanied by strong structural changes [10–12]. At the transition the  $c$  lattice parameter shrinks and in-plane parameters elongate, coupled with a transition from elongated  $\text{RuO}_6$  octahedra at high temperature to flattened octahedra in the insulating state. This seems to be the essential element to change the orbital occupation and to induce insulating behavior [13,14]. But upon cooling also the tilting of the  $\text{RuO}_6$  octahedra increases and the octahedron basal plane becomes elongated along the orthorhombic  $b$  direction [10–12]. This later distortion seems to pin the magnetic moment parallel to the  $b$  axis [15]. The strong structural changes are not restricted to the metal-insulator

transition at 357 K but extend over a large temperature interval down to about the onset of AFM order at  $T_N = 110$  K. Note, that  $\text{Ca}_2\text{RuO}_4$  is a layered material resulting in rather low three-dimensional AFM ordering temperatures.

Besides by heating, the metal-insulator transition can be induced by applying hydrostatic pressure above 0.5 GPa [12,16], by substitution, for example, with Sr [17] and by applying an electric field [18]. The electric field needed to drive the phase transition is unusually small ( $E = 40$  V/cm) compared to the Mott energy gap; it is about two orders of magnitude below a typical break-through field of a Mott insulator [19,20]. Following this discovery [18] several other studies confirmed current-induced quasimetallic states in  $\text{Ca}_2\text{RuO}_4$  [21–24]. In particular, by using a noncontact infrared thermometer it was shown that the metallic phase can be stabilized by an external current at a sample temperature well below the metal-insulator transition [23]. The low-temperature observation of the quasimetallic states suggests a truly electric mechanism and thus excludes Joule heating of the entire sample as the origin [21–23]. However, if the sample becomes inhomogeneous and splits in metallic and insulating parts the heating becomes inhomogeneous as well. Local heating remains a problematic issue in almost all experimental studies.

It was reported that  $\text{Ca}_2\text{RuO}_4$  exhibits strong diamagnetism and anomalous transport properties [21] at moderate current densities of 1 to 2 A/cm<sup>2</sup>. At low temperature the magnetoresistance turns negative and the Hall coefficient exhibits a sign change [21]. However, the evidence for strong diamagnetism was recently shown to arise from an experimental artifact [25]. Strong diamagnetism contrasts with the ferromagnetic or quasiferromagnetic instabilities reported for the metallic phases reached by applying pressure or by substitution [12,16,26,27].

For moderate current densities, nano-imaging optical techniques report nanostripe structured areas of phase

\*braden@ph2.uni-koeln.de

coexistence with different optical reflectivity [24]. This documents that the real structure of current carrying  $\text{Ca}_2\text{RuO}_4$  can be nonhomogeneous. Diffraction experiments at a high current density of  $10 \text{ A/cm}^2$  proposed new structural phases in a current carrying sample [28], but the crystal structures strongly resemble those  $\text{Ca}_2\text{RuO}_4$  exhibits at higher temperatures and pressure [10–12]. Other diffraction experiments on a crystal with 3% Mn substitution report evidence for a modified orbital arrangement [22]. The later study, furthermore, does not find any evidence for strong diamagnetism.

Here we report transport and single-crystal diffraction studies using neutron and x-ray radiation. The diffraction experiments with a careful recording of the sample temperature indicate complex phase coexistence of at least three different phases distinguished by different  $c$  lattice parameters. In particular, at low current densities, in addition to the initial metallic and insulating phases an additional component appears.

## II. EXPERIMENT

Single crystals of  $\text{Ca}_2\text{RuO}_4$  were grown by the floating-zone technique and characterized by resistivity and magnetization measurements [15,29]. Due to the metal-insulator transition at 357 K and the accompanied structural transition the crystals tend to shatter into mm-sized pieces upon cooling to room temperature in the furnace. A small amount of 1% Ti substitution broadens the transition, which can result in large single crystals of up to  $1 \text{ cm}^3$  volume. Additionally, and more importantly for this study, Ti-substituted crystals permit to pass the metal-insulator transition several times without destroying the sample. The magnetism is not strongly influenced by the Ti since it is isovalent to Ru and nonmagnetic [29]. In the experiments presented here crystals containing 1% of Ti and pure ones were used. For the application of the DC current in the quasistatic conductance and in the diffraction experiments, the plate-shaped crystals were glued to a copper plate using conductive silver paste. The  $ab$  planes are parallel to the plate. The copper plate as well as the sample were contacted with copper wires, resulting in a current direction parallel to the  $c$  axis. We choose this current direction because it offers the best conditions for thermalizing the sample thereby reducing heating issues. In addition, cracking of the sample in thin plates parallel to the current is suppressed.

Time-resolved pulsed transport measurements were performed in a high bandwidth coaxial setup suitable for frequencies up to the GHz range employing a current source KEITHLEY 2400 together with a 200 MHz oscilloscope AGILENT U2702A and a fast pre-amplifier STANFORDRESEARCH 560. The time-resolved temperature measurements were performed using a fast, thin ( $250 \mu\text{m}$ ) foil-type thermocouple [T-type] with a response time in the millisecond range. The sample was prepared as a small platelet with a thickness of 0.5 mm and a cross section of  $0.8 \text{ mm}^2$  covered with silver electrodes.

The x-ray diffraction (XRD) experiments were conducted on a D5000 powder diffractometer using  $\text{Cu K}\alpha$  radiation equipped with a He cryostat where the sample chamber is cooled by He flow. Thermal contact to the single crystalline samples is guaranteed by the exchange gas inside the chamber.

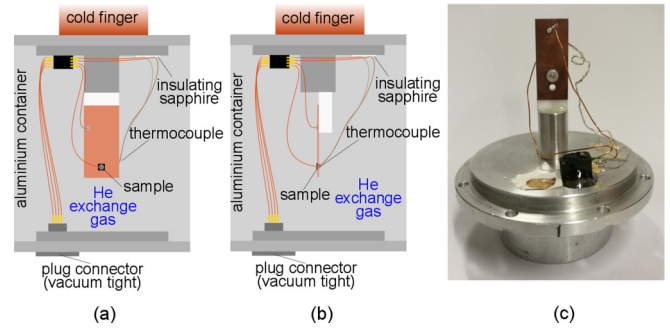


FIG. 1. Illustration of the experimental setup to perform x-ray and neutron diffraction experiments on  $\text{Ca}_2\text{RuO}_4$  with a current flowing parallel to the crystallographic  $c$  direction (perpendicular to the Ru layers). Note that the thermal couple opposite to the sample crystal allows for improved estimate of the sample temperature.

For the neutron diffraction experiments the sample setup was incorporated into a sealed aluminum can including He exchange gas and a vacuum tight connector. The can was then cooled using closed-cycle refrigerators. The elastic neutron scattering experiments were performed at the thermal two-axis diffractometer 3T1 at the Laboratoire Léon Brillouin (LLB). Neutrons with a wavelength of  $2.4 \text{ \AA}$  were extracted by a vertically focusing pyrolytic graphite (002) monochromator. To achieve the high resolution required to distinguish the different contributions in  $\text{Ca}_2\text{RuO}_4$  we used collimations of  $15'$  and  $10'$  before the monochromator and detector, respectively, and higher-order contaminations were suppressed with a pyrolytic graphite filter. To apply the current and to read the voltage generated by the thermocouple a KEITHLEY 2400 source meter and a KEITHLEY 2128 nanovoltmeter were used.

To monitor the sample temperature as exactly as possible in the neutron experiment one contact of a thermal couple was placed on the backside of the 0.5-mm-thick copper plate, precisely at the sample position. As the reference temperature of the thermocouple the cryostat sensor was used, so that we can precisely determine the temperature at the sample position. The experimental mounting used in most of the neutron experiments is shown in Fig. 1. In the x-ray diffraction experiment the thermocouple had to be mounted at the same side of the copper plate at a distance of 2 mm from the crystal.

## III. RESULTS

### A. Quasistatic transport studies of the insulator metal transition

Nakamura *et al.* [18] found that the insulator-metal transition in  $\text{Ca}_2\text{RuO}_4$  can be induced when applying an electric field of  $E = 40 \text{ V/cm}$  at room temperature. At this field the sample resistance drops leading to a jump in current density  $j$ . For the transport studies we use a two-contact circuit with a finite preresistance that limits the current when the samples becomes metallic, and we drive the sample with controlled voltage. In contrast, for the temperature-dependent diffraction studies we drive the crystal by controlling the current, as otherwise the current would strongly change with temperature. When ramping the current up in the current-controlled mode the electronics regulate the voltage to reach the demanded

current and initially exceeds the critical voltage or electric field and thus enforces the partial insulator-metal transition. We confirm the current-induced insulator-metal transition [18] in both samples, pure and Ti substituted ones, with critical electric fields of the same order (Fig. 2). The critical field denotes the value, at which the material changes from insulating to conducting characteristics. Upon cooling the sample resistivity increases and the critical electric field increases as well [Figs. 2(g) and 2(h)] similar to reports in Refs. [18,30]. The more insulating the sample becomes, the higher fields are necessary to transform it to the metallic state. For this reason any changes of current or voltage in the XRD and neutron experiments were applied above 250 K, where the samples are still conductive enough and where stronger cooling power is provided.

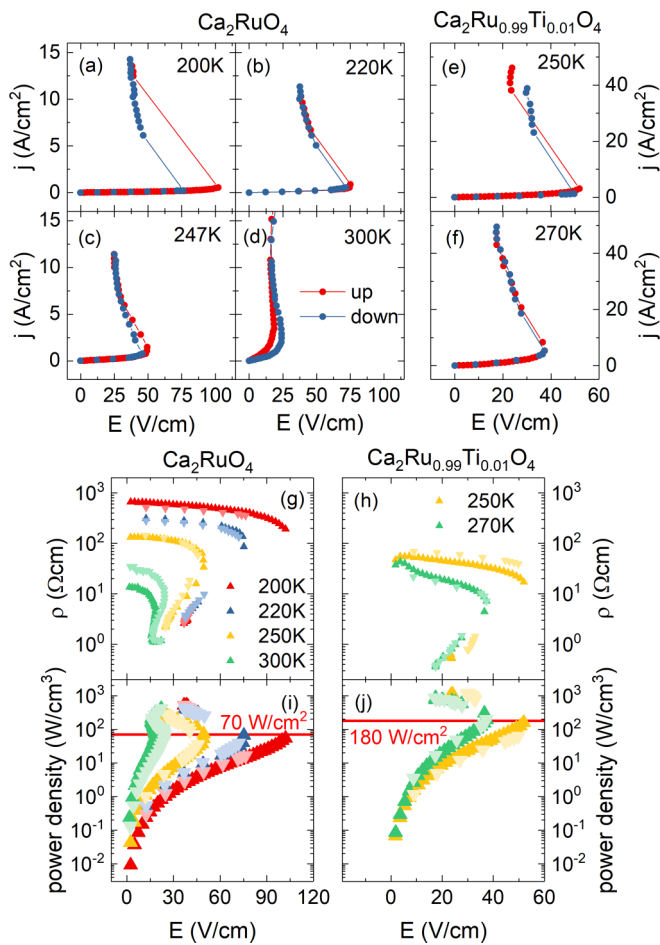


FIG. 2. Switching characteristics of pure and 1% Ti-substituted  $\text{Ca}_2\text{RuO}_4$  in dependency of temperature. (a)–(f) Characteristic  $j$ - $E$  curves display the current-induced phase transition in a voltage controlled setup (the electric field has been corrected for the circuit resistance effects). Here red coloring denotes data taken for ramping the voltage up and blue for ramping down. (g, h) The calculated resistivities from the two-point measurements above show a clear drop at a temperature-dependent critical electric field. (i) and (j) represent the corresponding power densities in the  $j$ - $E$  characteristic. The threshold power density, at which the switching occurs, is constant for all measured temperatures. Dark coloring is used for the up direction, light coloring for the down direction.

While the critical electric field increases, the critical current density decreases with decreasing temperature. The resulting critical power density does not exhibit a temperature dependence but stays constant for the measured temperature range between 220 and 300 K [Figs. 2(i) and 2(j)], which indicates that the current-induced insulator-metal transition is not simply due to heating of the entire crystal. Many aspects of the electric-field-driven insulator-metal transition in  $\text{Ca}_2\text{RuO}_4$  resemble that in  $\text{VO}_2$ , for which it was also reported that the threshold power density does not vary with temperature [31]. Both  $\text{Ca}_2\text{RuO}_4$  samples, pure and substituted ones, show comparable switching behavior. The substituted sample exhibits a slightly lower resistivity which is connected to higher critical current densities. The threshold electrical power density is therefore more than a factor of 2 higher than that in the pure sample [Figs. 2(i) and 2(j)]. Nevertheless the Ti substitution does not effect the current-induced insulator-metal transition significantly, for which reason the substitution can be disregarded for the following analysis of results.

The form of the  $j$ - $E$  characteristic, see Fig. 2, that has consistently been reported by many groups [18,23,30] inevitably leads to the formation of inhomogeneous current-carrying states. This effect has been shown on general grounds, and it is well known in the physics of semiconductors [32] that the state with negative differential resistance  $\frac{dj}{dV} < 0$  is absolutely unstable. Therefore, the  $S$ -shaped  $j$ - $E$  (or  $I$ - $V$ ) characteristic leads to the formation of filaments predominantly parallel to the current (but in the real system usually forming a percolation network), whereas the  $N$ -shaped  $I$ - $V$  curve results in the formation of insulating and metallic domains (Gunn domains) perpendicular to the current (Gunn domains usually move with current leading to the oscillating behavior—Gunn oscillations). The formation of metallic filaments in an insulating matrix is well documented in many systems with insulator-metal transitions, notably in  $\text{VO}_2$  [31,33–35] and in  $\text{SrTiO}_3$  [36]; they lead to a percolation picture of conduction and to switching phenomena. Due to the impact of strain, however, the arrangement of the metallic parts can essentially change, see discussion below.

As a result of the inhomogeneous state the current is predominantly concentrated in narrow metallic channels, in which the local current density is much higher than the average one, so that the local Joule heating  $jEV = \rho j^2$  (in the current-controlled regime, as used in most experiments) and the resulting local temperature in the current carrying parts will also be higher than that estimated by bulk probes. The question whether the metal-insulator switching often observed in systems with metal-insulator transition is due to intrinsic effects or caused by local heating is difficult to answer.

## B. Time-resolved analysis of the current-induced insulator-metal transition

To elucidate the question of what induces the rise in conductivity, the electric field connected to the forced current or simple Joule heating, we performed time-resolved pulsed experiments as illustrated in Fig. 3. Most likely one has to consider phase separation into an insulating and a percolating phase carrying most of the current. The idea of the time-resolved study is to disentangle timescales of a field-driven

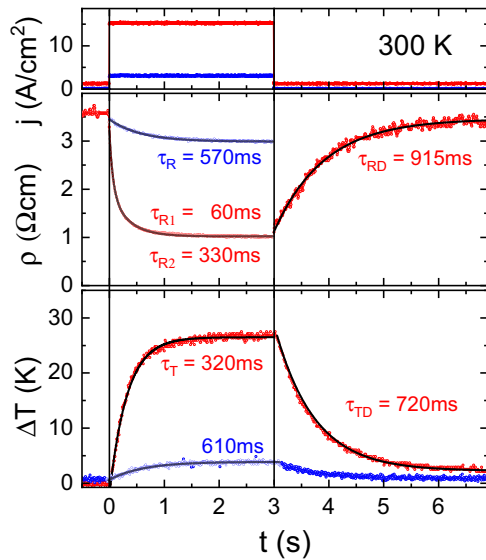


FIG. 3. Pulsed current measurements of sample resistivity (middle panel) and temperature (bottom) in  $\text{Ca}_2\text{RuO}_4$ . For driving currents below the threshold ( $3 \text{ A/cm}^2$ , blue, top panel) the resulting change in  $\rho$  can be modeled with an mono-exponential decay with a decay time similar to the rise time found for the concomitant heating (bottom panel). For larger driving currents above the threshold ( $15 \text{ A/cm}^2$ , red, top panel) the change in  $\rho$  only can be modeled employing a bi-exponential decay: A slowly relaxing component  $\tau_{R2} \approx 300 \text{ ms}$  in accord with the rise time of temperature (bottom) and a significantly faster process with  $\tau_{R1} \approx 60 \text{ ms}$ , which seems to be directly induced via the current, or correspondingly, via the electric field.

switching process and of presumably unavoidable heating effects.

The upper panel of Fig. 3 displays the pulse pattern used to induce additional conductivity. Switching-on a smaller current of about  $3 \text{ A/cm}^2$  leads to a mono-exponential drop in resistivity (middle panel) of about 15% with a slow time constant of  $\tau_R = 570 \text{ ms}$ . At the same time the sample temperature rises with a similar time constant saturating 3.2 K above the starting value of 298 K. Obviously, the resistivity changes in this below-threshold regime are coupled to the heating. After switching-off the current at  $t = 3 \text{ s}$  the temperature decays to 298 K again. Considering a power dissipation of about  $\rho j^2 \approx 15 \text{ W/cm}^3$ , and thus still of the order of 6 mW in the sample crystal even for this smaller driving current, such heating has to be expected. The red curves in Fig. 3 denote results for the larger driving current of  $15 \text{ A/cm}^2$ . Here a small base current of  $1 \text{ A/cm}^2$  is applied before and after the pulse to enable the determination of the resistivity in these regimes. The drop in resistivity now amounts up to 70% but it is not possible to describe the underlying time dependence using only one relaxation time. A bi-exponential fit reveals a much faster decay time of  $\tau_{R1} \approx 60 \text{ ms}$ , together with a slower one of  $\tau_{R2} \approx 330 \text{ ms}$ . This last is in accord with the corresponding rise time of the temperature (bottom). The faster process seems not to be induced by simple heating (even though a considerable increase in temperature of up to 28 K can be monitored). This second mechanism has to be attributed to the direct induction of a more conductive phase

via the current or, correspondingly, via the electric field. It is interesting to note that after switching-off this larger driving current, the electrical relaxation time exceeds the thermal one. The field-induced phase appears to be metastable which is in accord with the observed hysteresis in the  $j$ - $E$  curves, see [18] and Fig. 2.

The observation of two relaxation rates in the resistance unambiguously confirms an intrinsic origin of the current induced switching. There are several processes that can be associated with the faster conductance enhancement, such as a purely electronic mechanism or filament formation. The fact that even this faster process happens on a timescale above milliseconds suggest some structural implication.

### C. X-ray and neutron diffraction studies as function of current density and temperature

Since the metallic and insulating phases in  $\text{Ca}_2\text{RuO}_4$  differ strongly in their lattice constants, diffraction is a suitable experimental technique to investigate phase changes in this material. Specifically, the lattice parameter  $c$  strongly increases by  $\approx 3\%$  between the insulating phase at room temperature and the metallic phase at  $\sim 360 \text{ K}$  [10,11], which allows one to distinguish these two phases. However, a good resolution is required in neutron diffraction experiments. One expects to observe (00L) reflections at lower  $2\theta$  values when the material becomes metallic. The metallic phase (MP) of  $\text{Ca}_2\text{RuO}_4$  was initially labeled as  $L$  phase due to its longer  $c$  axis, while the insulating phase (IP) is frequently labeled as  $S$  (for short) phase [7,10].

As described above, switching the  $\text{Ca}_2\text{RuO}_4$  crystals from the insulating to the metallic state involves large power densities. Note that a power density of  $100 \text{ W/cm}^3$  would result in a temperature drift of 36 K/s for a material without any thermal contact just by taking the specific heat into account [37]. As illustrated in the time-resolved experiments, heating of the sample during the diffraction studies cannot be completely avoided and must be carefully taken into consideration. The controversial diffraction results [18,22,28,30] most likely stem from differing heating conditions. With an additional sensor placed close to the crystal and with the good electric and thermal contact of the sample to a large Cu plate heating effects could be reduced and better documented in most of our experiments.

As a first example, we show the ramping up of the current density in a neutron diffraction experiment in Fig. 4. The cryostat temperature was set to 250 K, which is advantageous compared to simple experiments at ambient conditions because it provides strong cooling power. The thermocouple with its sensor placed opposite to the crystal on the Cu plate shows that heating occurs even at these rather low current densities. Note that the thermocouple can only give a lower estimate of the true sample temperature. Similar to several other studies we observe an increase of the  $c$  lattice parameter of the insulating phase. Half of this can be attributed to the temperature change detected in the thermal couple and thus to heating of the entire sample, but most likely an even larger part of the  $c$  parameter enhancement is simply due to heating. In the scenario of phase separation the metallic parts will sense even higher local heating.

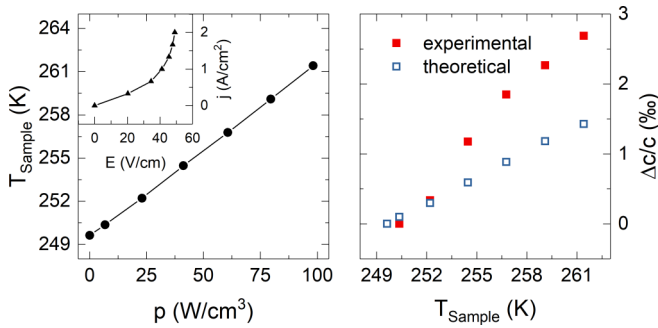


FIG. 4. Sample temperature (thermocouple) in comparison to power density and relative lattice change while ramping up current at the fixed cryostat temperature of 250 K. The purely temperature-driven relative lattice change (open squares) is taken from Ref. [11] for the given temperature range. The experimental lattice change is derived from the (006) reflection in the neutron diffraction experiment.

Some studies seem to partially ignore the heating and report an important intrinsic change of the insulating phase with small currents, a modified short- $c$  phase. However, this modified short- $c$  phase in Ref. [28] exhibits a  $c$  lattice constant increase just up to the maximum value that the insulating  $\text{Ca}_2\text{RuO}_4$  phase reaches upon heating without a current (before the insulator-metal transition takes place at 357 K). Furthermore, the modified short- $c$  phase proposed at 130 K with a large current density of  $10 \text{ A}/\text{cm}^2$  perfectly agrees with the current-free insulating phase at the temperature of 240 K: The lattice constants reported in Ref. [28] amount to  $a = 5.404$ ,  $b = 5.547$ , and  $c = 11.848 \text{ \AA}$  compared to  $a = 5.407$ ,  $b = 5.560$ , and  $c = 11.854 \text{ \AA}$  for current-free  $\text{Ca}_2\text{RuO}_4$  at 240 K, taken from Ref. [11], and also the internal parameters perfectly agree [38].

XRD experiments with a Ti-free sample show a second (002) reflection appearing when the current density is increased to  $j = 69 \text{ A}/\text{cm}^2$  at a temperature of 294 K [Fig. 5(a)]. Note, however, that the sample was already mounted into a cryostat and temperature stabilized in order to reduce the local heating. The characteristic  $j$ - $E$  curve [Fig. 5(c)] and the resistivity [Fig. 5(e)] indicate that the sample becomes already conductive at much lower current densities ( $\approx 2.6 \text{ A}/\text{cm}^2$ ), where no significant change in the diffraction pattern is observable [Fig. 5(a)]. At high temperature, the Bragg reflection associated with the metallic phase exhibits a similar intensity as that of the insulating phase, but it becomes rapidly weaker upon cooling [Figs. 5(b) and 5(d)] in spite of the rather large current flowing. The  $c$  lattice parameter of the metallic phase stays constant upon cooling in agreement with measurements on Sr-substituted materials, in which the metal-insulator transition occurs at lower temperatures [11] [Fig. 5(f)]. The  $2\theta$  value of the Bragg peak associated with the insulating phase increases upon cooling following the pronounced shortening of the  $c$  lattice parameter of the insulating phase at low temperature. The cryostat temperature has been corrected by the offset indicated by the thermal couple scaled by a factor of 2.5 to take the slight displacement of the thermocouple in the x-ray diffraction experiment into account. Nevertheless the observed  $c$

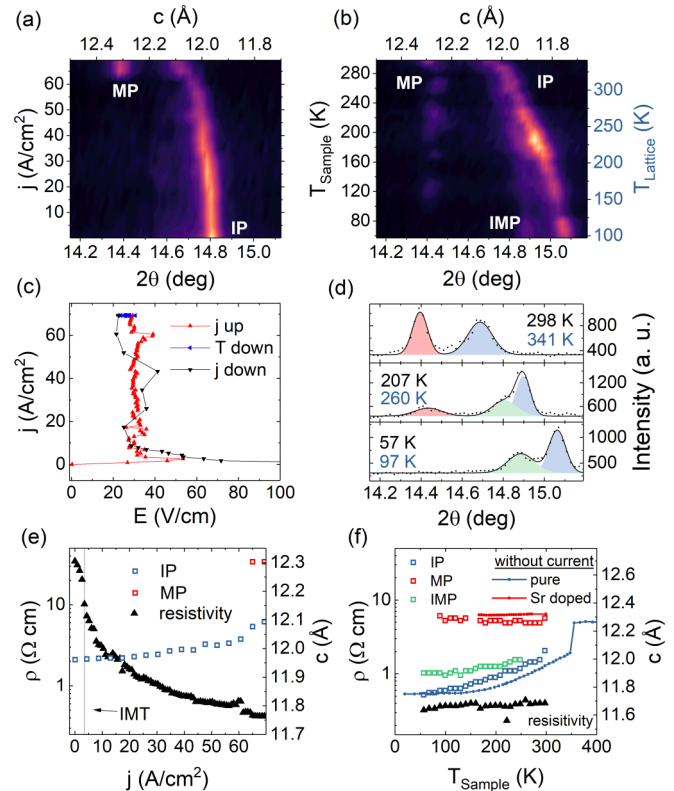


FIG. 5. X-ray diffraction study of the (002) reflection under an applied current density of up to  $j = 69 \text{ A}/\text{cm}^2$  on pure  $\text{Ca}_2\text{RuO}_4$ . Panels (a) and (b) show the evolution of different phases characterized by different  $c$  lattice parameters while ramping up current and cooling down with constant current, respectively. The coexistence of phases, visible in the three reflections, is strongly temperature dependent. (c) The  $j$ - $E$  curve is measured simultaneously to the XRD experiment while ramping up current, cooling down, and decreasing the current. (d) The quantitative analysis of  $2\theta$  scans clearly displays the phase mixture of three phases. Here the metallic (MP) and insulating (IP) phases are colored in red and blue, respectively. The third phase is colored in green and is labeled as intermediate phase (IMP).  $T_{\text{Sample}}$  (black) represents the cryostat temperature corrected by the thermocouple while  $T_{\text{Lattice}}$  (blue) is calculated by comparing the reflection angle of insulating phase to the temperature dependency of a current free sample, taken from Ref. [11], i.e., ignoring any intrinsic change. (e, f) Resistivity and lattice parameter in dependence to current density and sample temperature, respectively. The resistivity displays the occurrence of the insulator-metal transition long before the metallic phase becomes visible in (e) the XRD measurement and (f) the decreasing resistivity while cooling down coincides with the phase existence of the intermediate phase. The temperature dependency of  $c$  lattice parameter of  $\text{Ca}_2\text{RuO}_4$ , from Ref. [11], is added for comparison. The low-temperature lattice parameter of the metallic phase (red line) is taken from data of  $\text{Ca}_{1.9}\text{Sr}_{0.1}\text{RuO}_4$  from the same reference.

values of the insulating phase lie above the reported temperature dependence of the insulating phase without any current [Fig. 5(f)]. At high temperature, the insulating phase reflection exhibits significant broadening, see Fig. 5(d), which can be easily recognized from the comparison with the metallic phase peak [Fig. 5(d)]. Below  $\sim 260 \text{ K}$  a third reflection appears

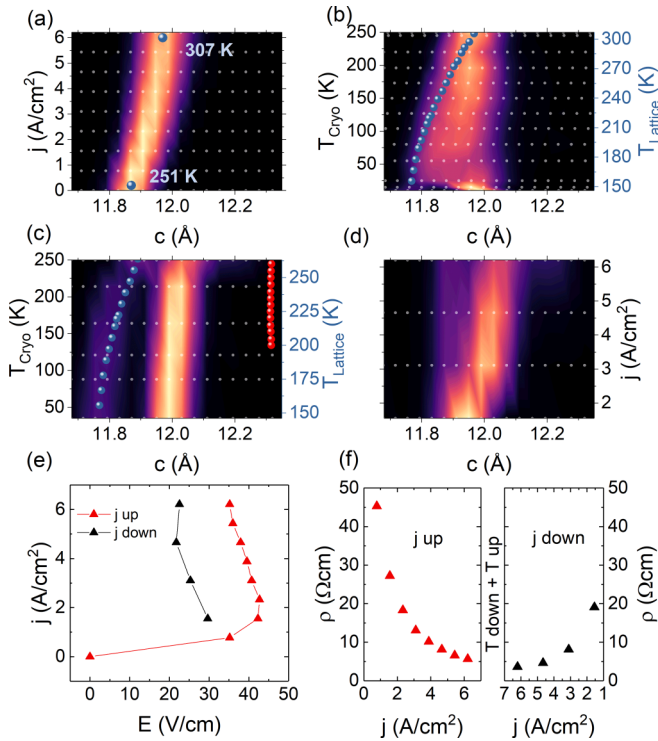


FIG. 6. Evolution of  $c$  lattice parameter recorded by elastic neutron scattering in a measuring sequence of (a) increasing current, (b) decreasing temperature, (c) increasing temperature, and (d) decreasing current. Longitudinal scans are taken across the (006) reflection in pure  $\text{Ca}_2\text{RuO}_4$  at various current densities and temperatures. The blue circles represent the temperature dependency of  $\text{Ca}_2\text{RuO}_4$  lattice parameters without current, taken from Ref. [11] and is used to determine  $T_{\text{Lattice}}$  from the experimental lattice parameter of the insulating phase. The low-temperature lattice parameter of the metallic phase (red balls) is taken from data of  $\text{Ca}_{1.9}\text{Sr}_{0.1}\text{RuO}_4$  from the same reference and plotted against  $T_{\text{Lattice}}$ . The small gray dots represent the measured points and the color maps are obtained with an interpolation algorithm. (e) The  $j$ - $E$  curve is measured simultaneously to the neutron diffraction experiment while ramping up current, cooling down, heating up, and decreasing the current. (f) Sample resistivity is derived from the two-point measurement and displayed for the measurement sequence.

that unambiguously indicates phase coexistence of at least three phases with different  $c$  lattice parameters: Besides the insulating phase (IP) and the metallic phase (MP) there is an intermediate phase (IMP), see Fig. 5(d).

The coexistence of three phases is confirmed by neutron diffraction experiments which also aim to characterize the magnetic ordering in the low current-density range. In a first set of experiments (Fig. 6) the current density was ramped up to  $j = 6.2 \text{ A/cm}^2$ . An additional thermocouple could not be used in this experiment. The color maps in Figs. 6(a) to 6(d) represent the lattice parameter  $c$  extracted from longitudinal scans across the (006) Bragg position and its change during a full measurement cycle of ramping up the current, cooling, reheating, and ramping the current down. At a cryostat temperature of 250 K the current increase leads to an increased  $c$  lattice parameter while no additional reflection becomes visible [Fig. 6(a)]. The  $j$ - $E$  curve clearly

indicates a transition from insulating to metallic state at only  $j = 1.55 \text{ A/cm}^2$ , see Fig. 6(f). The shift of the insulating phase reflection can mostly be assigned to a thermal drift of the sample and therefore it can be used to roughly estimate the sample temperature, although this will overestimate the temperature due to the neglecting of the intrinsic shift, see discussion below. A current density of  $j = 6.2 \text{ A/cm}^2$  heats up the sample by  $\sim 50 \text{ K}$ . When cooling the sample under fixed current a phase separation at low temperatures occurs similar to the XRD observation. The significant broadening of the insulating phase peak increases until two reflections can be distinguished, which we assign to the insulating phase and the intermediate phase [Fig. 6(b)]. Interestingly this phase segregation is not reversible as the two distinct reflections stay separated when increasing the temperature again, see Fig. 6(c). The phase separation and the appearance of the intermediate phase is associated with a reduction of the resistance, see Figs. 6(e) and 6(f), which also reduces the sample heating. Therefore, the sample temperature with the cryostat stabilized at 250 K is lower after the cooling and heating cycle. In addition to the insulating and intermediate phase reflections a weak third peak becomes visible at high temperatures with a  $c$  lattice parameter close to the metallic phase. This third phase also disappears quickly when reducing the current density at  $T_{\text{cryo}} = 250 \text{ K}$  at the end of the full cycle. Below  $3 \text{ A/cm}^2$  the intermediate phase reflection fades out and only one reflection persists [Fig. 6(d)]. The presented full measurement cycle documents a complex real structure arising from phase segregation with strong hysteresis. The amount of insulating, intermediate and metallic phase are not only determined by current strength and temperature but also depend on the history of the sample, similar to reports in Ref. [22].

The mappings of the reflection against longitudinal (00 $\xi$ ) and transversal ( $\xi 00$ ) directions clearly reveal the phase coexistence (see Fig. 7). At high current densities the phase separation is already visible at high temperatures whereas at low current densities the coexistence only appears at low temperatures. It can be concluded that the samples show more than the two conventional insulating and metallic phases at low temperatures. The different positions of the Bragg peaks in the transverse direction (see Fig. 7) indicate that the different lattices are slightly tilted against each other similar to ferroelastic domains in a martensitic transition, see, e.g., Refs. [39,40].

Using a two-axis diffractometer the accessible  $Q$  space is limited to a scattering plane spanned by two crystallographic directions. Therefore, a full structural analysis is not possible. But the twinning of the crystals with respect to the orthorhombic distortion allows one to measure the (200) and (020) reflections in addition to the (006) reflection [Fig. 8(a)]. In this set of neutron experiments with a stronger closed cycle refrigerator SUMITOMO RDK 205D and with a thermocouple mounted as indicated in Fig. 1, we cooled the crystal with a further reduced current density of  $j = 1.5 \text{ A/cm}^2$ . We find qualitatively the same phase segregation and the appearance of the intermediate phase reflection below  $\sim 50 \text{ K}$ , as it is shown in the longitudinal scan across the (006) Bragg position, see Fig. 8(a). The longitudinal scans across (200) show two reflections. The  $a$ -axis twin results in higher  $2\theta$  values

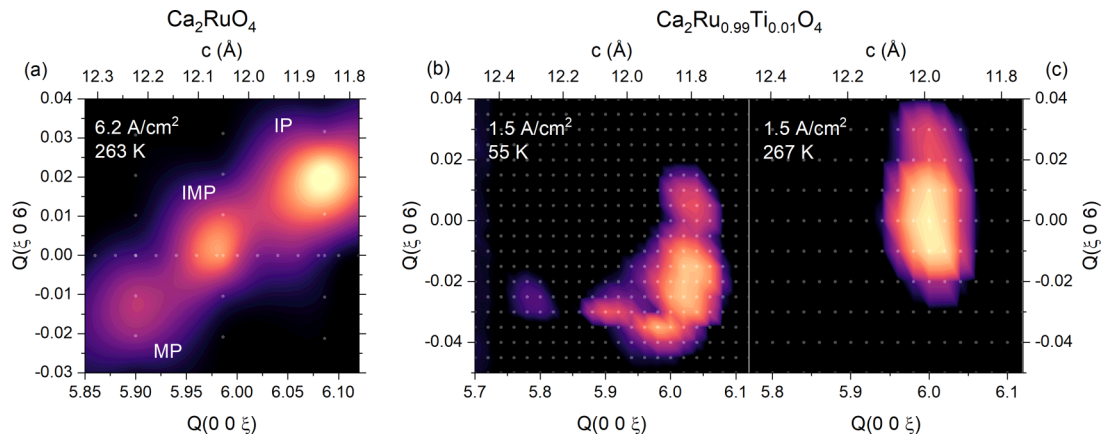


FIG. 7. Mapping of reflections around (006) Bragg peak for two different samples, temperatures, and current densities. The small gray dots represent the measured points and the color maps are obtained with an interpolation algorithm.

and the *b*-axis twin in lower values, respectively, because the lattice parameter *a* is smaller than *b*. The *a*-axis peak does not exhibit a strong temperature dependence, neither in  $2\theta$  nor in peak width. However, the *b*-axis reflection shifts to higher  $2\theta$  values synonymous with the decrease of the lattice parameter *b*. Only at 39 K the lattice parameter *b* increases again. Additionally to the shift, the Bragg peak of the *b*-axis twin is significantly broadened below 50 K [Fig. 8(c)]. This broadening can be attributed to the appearance of the intermediate phase, whose *b* lattice parameter is expected to be slightly smaller since it exhibits a more metallic character. Both the appearance of the intermediate phase and the broadening of the *b*-axis reflection below 50 K, coincide with a drop in sample re-

sistance [Figs. 8(b) and 8(c)]. This again connects the appearance of the intermediate phase to an increased conductivity.

Sow *et al.* showed that below 50 K  $\text{Ca}_2\text{RuO}_4$  exhibits anomalous properties under applied current [21]. In their magnetization measurements they could not find any anti-ferromagnetic transition for nonzero current densities. Ti-substituted  $\text{Ca}_2\text{RuO}_4$  exhibits the B-centered AFM order [29], which leads to a magnetic (101) Bragg reflection [29]. We studied this reflection depending on temperature and under applying a small current density (Fig. 9). Without current application the peak intensity rapidly decreases only close to the transition temperature  $T_N = 110$  K and becomes zero already at 119 K [Fig. 9(a)]. Single point counts on the

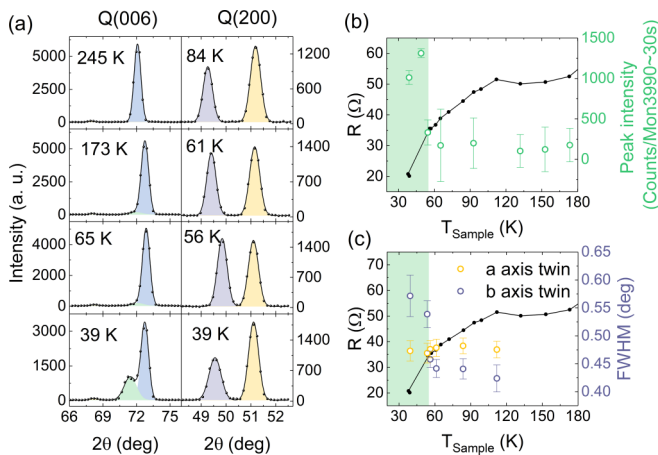


FIG. 8. (a) Longitudinal scans across the (006) Bragg peak, left column, and (200) Bragg peaks, right column, at various temperatures and with applied current ( $j = 1.5 \text{ A/cm}^2$ ) on pure  $\text{Ca}_2\text{RuO}_4$ . The black line represents the sum of Gaussians while the single contributions are marked by the colored areas. In the left column the blue area illustrates the metallic phase, green the intermediate phase whereas the different twin fractions visible in the longitudinal scans of (200) are displayed in yellow (*a* axis twin) and purple (*b* axis twin). (b) Comparison of the temperature dependence of the sample resistance and the fitted peak intensity of intermediate phase. (c) Comparison of the temperature dependence of the resistance and the fitted peak width of both twin fractions.

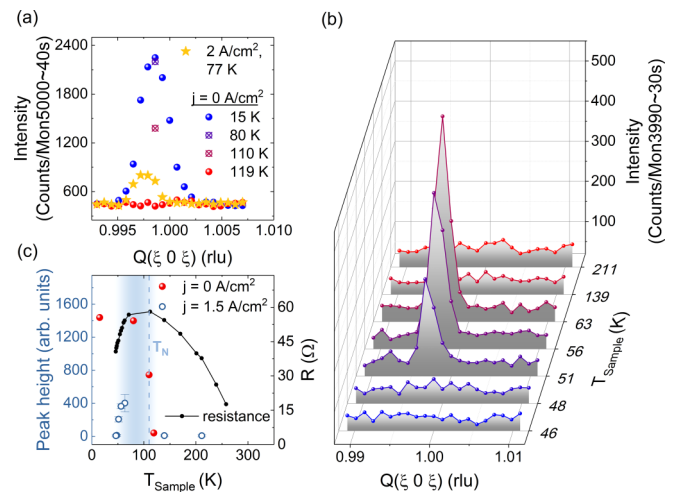


FIG. 9. Influence of current application on the magnetic (101) reflection in substituted  $\text{Ca}_2\text{RuO}_4$ . (a) Longitudinal scans over (101) and single-point count rates at different temperatures. The magnetic signal is reduced but persists with a low current density of  $j = 1.5 \text{ A/cm}^2$ . (b) Temperature dependence of longitudinal scans over the (101) reflection with an applied current density of  $j = 1.5 \text{ A/cm}^2$ . (c) Temperature dependence of the sample resistance recorded simultaneously with the neutron scattering in comparison to the peak heights from panel (b) (obtained by fitting with Gaussians). The red spheres represent the peak height of the (101) reflection measured without current from panel (a).

maximum of the longitudinal scan over (101) at 80 K show that the intensity has little changed up to this temperature in agreement with previous reports [10,29]. While applying a current of 120 mA ( $j = 2 \text{ A/cm}^2$ ) the lowest sample temperature reached is 70 K as determined by the thermocouple. At this experimental configuration ( $T_{\text{sample}} = 77 \text{ K}$ ,  $j = 2 \text{ A/cm}^2$ ) the (101) reflection remains visible, although with reduced intensity compared to the current-free phase at 80 K. It can be clearly stated that magnetically ordered regions survive the application of small currents. The reduction of peak intensity can be caused by various factors such as reduction of ordered phase volume or reduction of the transition temperature and ordered moment. By applying lower current densities ( $j = 1.5 \text{ A/cm}^2$ ) it is possible to cool the sample below 50 K (as indicated by the thermocouple), see Fig. 9(b) for the temperature-dependent evolution of the (101) reflection. The peak intensities in Fig. 9(c) reflect the appearance of the magnetic Bragg peak at 63 K, well below the transition temperature of current free  $\text{Ca}_2\text{RuO}_4$ . Surprisingly the Bragg peak at the magnetic position does not persist to low temperatures but suddenly disappears upon further cooling. The suppression of the AFM ordering can be associated with the appearance of the intermediate phase and the reduction of the resistance, see Figs. 8 and 9.

#### IV. DISCUSSION

The totality of diffraction studies in our and in previous [18,22,28,30] experiments remains puzzling and cannot be fully reconciled. Most likely different experimental conditions—in particular concerning temperature control and measurement—have a large impact on the real structure of the  $\text{Ca}_2\text{RuO}_4$  crystals that carry finite current density below the metal-insulator transition. Our comprehensive diffraction studies indicate that for the largest part of the studied current and temperature ranges the samples are structurally inhomogeneous presenting a complex phase coexistence. Phase coexistence must even be expected in view of the  $S$ -shaped  $j$ - $E$  characteristics [32].

Our experiments for currents perpendicular to the planes as well as all previous experiments agree concerning the fact that only very high current densities applied at elevated temperature result in strong Bragg scattering that can be associated with the high-temperature metallic state of  $\text{Ca}_2\text{RuO}_4$ , i.e., a  $c$  lattice constant close to  $12.25 \text{ \AA}$ . When ramping up a high current density of the order of  $j = 10 \text{ A/cm}^2$  and above, it seems unavoidable to heat the crystal and several groups report that the  $c$  value of the insulating phase increases close to  $\sim 12.05 \text{ \AA}$  [18,22,28], which is the largest  $c$  value the insulating phase of  $\text{Ca}_2\text{RuO}_4$  attains upon heating (without current) before it transforms to the metallic phase [11]. Even though there is no doubt that metallic conduction is induced at temperatures well below the metal-insulator transition as can be seen in, e.g., our time-resolved studies, any results with large current densities have to be considered with great care. Our temperature-dependent measurements at large current densities unambiguously show that even in this case the metallic phase Bragg contributions rapidly diminish upon cooling, see Figs. 5(a), 5(b), 5(d), and Fig. 6(c). When analyzing the total scattering one must, however, keep the spatial extension

of the different phases in mind. If the spatial extension of the metallic phase falls below the coherence length of the diffraction experiment, the metallic phase scattering will become broadened in  $Q$  space. For our XRD experiment with a conventional x-ray tube we can estimate the spatial coherence to be in the range of 40 nm [41], while the coherence length in the neutron experiments amounts to around 20 nm. In our and all previous diffraction studies the use of tiny crystals [18,22,28] rendered it impossible to characterize such weak diffuse scattering.

The low-current state in  $\text{Ca}_2\text{RuO}_4$  exhibits a large negative magnetoresistance [21] that is difficult to explain without magnetism. However, a similar observation in an imperfect bulk-insulating topological insulator was attributed to the Zeeman effect on barely correlating current paths [42].

Small metallic phase regions embedded in an insulating matrix will nevertheless impact the Bragg scattering of the insulating phase because the average  $c$  lattice constant within the coherence volume increases. Such effects can explain the behavior of the Bragg contributions of insulating and intermediate phases. The  $c$  constant of the insulating phase with finite current is very close to that of the current-free insulating phase, and the small deviations can stem from some current-induced heating combined with the admixture of short-range (i.e., extension below the coherence length) metallic parts, but the diffraction studies cannot exclude an intrinsic effect due to, e.g., homogeneous loss of orbital polarization. In particular, when ramping the current density up the inclusion of more and more metallic phase regions yields a continuous increase of  $c$ . The crystal structure reported for a large current density of  $10 \text{ A/cm}^2$  at 130 K [28] exactly corresponds to that of current-free  $\text{Ca}_2\text{RuO}_4$  at 240 K [11,38], therefore it can also be explained by metallic admixtures (combined with heating). However, the density functional theory (DFT) analysis proposing this structure as semimetallic [28] can be questioned in view of the well established insulating properties of  $\text{Ca}_2\text{RuO}_4$  at 240 K.

In pure and in substituted crystals we find the intermediate phase under various conditions, and evidence for a similar phase can also be found in the room temperature x-ray studies by Cirillo *et al.* [30]. The intermediate phase appears to be crucial for the understanding of the anomalous properties at low current densities, which must result from some important intrinsic change. Our neutron experiments for current densities of 1 to  $2 \text{ A/cm}^2$  suggest that the intermediate phase appears or becomes enhanced in the temperature range below 100 K. In addition we still find Bragg scattering at the position where AFM order contributes a Bragg peak in the normal insulating state. This observation indicates that AFM ordering can coexist with current carrying parts in one crystal, see Fig. 9. However, the AFM Bragg scattering disappears when the intermediate phase forms. Most likely the intermediate phase represents a more regular and more homogeneous arrangement compared to the modified insulating phase, but again a homogeneous loss of electronic order cannot be excluded on the basis of the diffraction studies. In the percolative picture of small metallic phase regions in an insulating matrix the intermediate phase is attributed to a stronger and more homogeneous content of metallic



regions with most likely also a more regular arrangement. The occurrence of the intermediate phase is accompanied with an enhanced conductance in agreement with a more regular arrangement.

The optical room-temperature studies by Zhang *et al.* [24] reveal a regular microstripe pattern of metallic phase and insulating phase regions. Such a regular arrangement is common in martensitic phase transitions that create strong local strain [39,40,43–45]. In martensite transitions the domains may even form well-defined superstructures [40,46] arising from a regular arrangement of very small domain sizes causing superlattice reflections. A similar strain mechanism was also proposed to explain stripe-like phenomena in various transition-metal oxides [47]. Indeed the differences in the lattice constants between metallic phase and insulating phase in  $\text{Ca}_2\text{RuO}_4$  without currents are huge. And these differences strongly increase upon cooling. The low-temperature  $c$  parameter of insulating  $\text{Ca}_2\text{RuO}_4$  is  $\sim 0.5$  Å shorter than that of the metallic phase, and the difference in the orthorhombic  $b$  parameter amounts to  $\sim 0.25$  Å. In contrast the  $a$  parameter is almost identical. The optical experiment examines an  $a$ ,  $b$  surface and finds stripes perpendicular to orthorhombic  $b$ , which is the expected arrangement for martensitic domains that reduce the strong in-plane strain along  $b$ . Similar domain arrangements must, however, also exist perpendicular to the planes, as the  $c$  strain would be even larger. Both strain effects should result in a relative tilting of metallic phase and insulating phase domains. Since the relative strains will increase by a factor of 3 upon cooling, the microstripe pattern will considerably change. The lattice strain seems to be the driving force for the rearrangement of the phase volumes and in particular for the occurrence of the intermediate phase at low temperatures. We speculate that the intermediate phase is a more fine mesh of insulating and metallic parts, so that the average is better defined with intermediate lattice constants. For this finer mesh there is enhanced mutual influence of one state on the other state, which explains the disappearance of AFM ordering. However, studies with local probes are required to fully resolve the structural nature of the intermediate phase. Considering the strain effects and the fact that the insulator-metal transition can be induced by only moderate hydrostatic pressure above 0.5 GPa [12,16], one may assume that  $\text{Ca}_2\text{RuO}_4$  grown on a substrate causing tetragonal strain will even more easily undergo the insulator-metal transition at low temperature.

It also appears most important to understand the relation between the two mechanisms explained above: The formation of conducting filaments typically parallel to the current arising from the general phase instability [32] and the impact of the crystal strain due to the large differences in lattice constants that will also favor domain formation similar to the well-known effects in martensite transitions [39,40]. One may only speculate how these two phenomena actually couple: under the influence of current, in a negative part of the  $j$ - $E$  curve of Fig. 2, the system becomes unstable. It first tends to form conducting filaments predominantly parallel to the current, in which the insulator-metal transition and local heating imply strong structural changes. But then the strong strain imposes its own pattern in this inhomogeneous state leading to the formation of more complicated microstructures, with metallic

inclusions not just parallel to the current, but largely determined by strain. Therefore, the current has to meander, which finally leads to percolating network. The general picture of the origin and of the main characteristics of the current carrying state in  $\text{Ca}_2\text{RuO}_4$  are certainly related to both mechanisms.

## V. CONCLUSION

X-ray and neutron diffraction studies as a function of temperature and applied current density reveal a complex real structure indicating that phase segregation and phase coexistence are essential for the physics of the current carrying state in  $\text{Ca}_2\text{RuO}_4$ . Evidence for phase segregation is deduced from the S-shaped quasistatic  $j$ - $E$  curves and from two distinct timescales visible in pulsed transport measurements. When crystals are cooled with controlled current density we observe three different contributions to the Bragg peaks that can be easily assigned to phases with distinct  $c$  lattice parameters. Except at very high current densities and at elevated temperatures, there are only minority phases corresponding to the high-temperature metallic state of  $\text{Ca}_2\text{RuO}_4$  with  $c$  lattice constants of the order of 12.25 Å. The relative weight of these metallic contributions to the Bragg scattering continuously decreases upon cooling. The suppression of the Bragg peaks associated with the long- $c$ -axis metallic state, however, does not exclude the persistence of such regions. The spatial extent of metallic regions can just become considerably lower than the coherence length of the diffraction experiment (of the order of 20 to 40 nm). For the lower current densities, below  $j = 2$  A/cm<sup>2</sup>, for which anomalous low-temperature properties have been reported, metallic long- $c$  Bragg scattering is irrelevant. The two other Bragg scattering contributions correspond to  $c$  lattice parameters close to the much smaller values expected for the insulating state. One phase, labeled insulating phase, exhibits rather similar though significantly larger  $c$  values compared to the current-free insulating state, while an intermediate contribution, intermediate phase, appears with about  $\sim 0.1$  Å larger  $c$  constants. Upon cooling, heating, and ramping the current densities up or down the phase ratio between insulating and intermediate states considerably varies, which is associated with changes in the resistance. Most importantly, we find evidence for AFM ordering even in samples carrying moderate current densities, but this AFM ordering seems to be suppressed when parts of the sample transform to the intermediate state.

The characters of the insulating and intermediate phases in the current carrying states cannot yet be fully established, but it cannot be excluded that they simply arise from phase coexistence and regular microarrangements of metallic and insulating regions. The general tendency to phase segregate and the impact of the local strain are proposed to drive the complex real structure in current carrying  $\text{Ca}_2\text{RuO}_4$  at low temperature.

## ACKNOWLEDGMENTS

This work was funded by the Deutsche Forschungsgemeinschaft (DFG, German Research Foundation) Project No. 277146847 - CRC 1238, projects A02, B02, and B04.

- [1] F. Chudnovskiy, S. Luryi, and B. Spivak, Switching device based on first-order metal-insulator transition induced by external electric field, in *Future Trends in Microelectronics: The Nano Millennium* (Wiley, New York, 2002), p. 148.
- [2] C. Vaju, L. Cario, B. Corraze, E. Janod, V. Dubost, T. Cren, D. Roditchev, D. Braithwaite, and O. Chauvet, Electric-pulse-driven electronic phase separation, insulator-metal transition, and possible superconductivity in a mott insulator, *Adv. Mater.* **20**, 2760 (2008).
- [3] M. M. Qazilbash, M. Brehm, B.-G. Chae, P.-C. Ho, G. O. Andreev, B.-J. Kim, S. J. Yun, A. V. Balatsky, M. B. Maple, F. Keilmann, H.-T. Kim, and D. N. Basov, Mott transition in VO<sub>2</sub> revealed by infrared spectroscopy and nano-imaging, *Science* **318**, 1750 (2007).
- [4] A. S. McLeod, E. Van Heumen, J. G. Ramirez, S. Wang, T. Saerbeck, S. Guenon, M. Goldflam, L. Andregg, P. Kelly, A. Mueller, M. K. Liu, I. K. Schuller, and D. N. Basov, Nanotextured phase coexistence in the correlated insulator V<sub>2</sub>O<sub>3</sub>, *Nat. Phys.* **13**, 80 (2017).
- [5] J. Jeong, N. Aetukuri, T. Graf, T. D. Schladt, M. G. Samant, and S. S. P. Parkin, Suppression of metal-insulator transition in VO<sub>2</sub> by electric field-induced oxygen vacancy formation, *Science* **339**, 1402 (2013).
- [6] K. Szot, R. Dittmann, W. Speier, and R. Waser, Nanoscale resistive switching in SrTiO<sub>3</sub> thin films, *Phys. Status Solidi RRL* **1**, R86 (2007).
- [7] S. Nakatsuji, S.-I. Ikeda, and Y. Maeno, Ca<sub>2</sub>RuO<sub>4</sub>: New Mott insulators of layered ruthenate, *J. Phys. Soc. Jpn.* **66**, 1868 (1997).
- [8] S. Nakatsuji, T. Ando, Z. Mao, and Y. Maeno, Metal insulator transition in Ca<sub>2-x</sub>Sr<sub>x</sub>RuO<sub>4</sub>, *Physica B* **259-261**, 949 (1999).
- [9] C. S. Alexander, G. Cao, V. Dobrosavljevic, S. McCall, J. E. Crow, E. Lochner, and R. P. Guertin, Destruction of the Mott insulating ground state of Ca<sub>2</sub>RuO<sub>4</sub> by a structural transition, *Phys. Rev. B* **60**, R8422(R) (1999).
- [10] M. Braden, G. André, S. Nakatsuji, and Y. Maeno, Crystal and magnetic structure of Ca<sub>2</sub>RuO<sub>4</sub>: Magnetoelastic coupling and the metal-insulator transition, *Phys. Rev. B* **58**, 847 (1998).
- [11] O. Friedt, M. Braden, G. André, P. Adelmann, S. Nakatsuji, and Y. Maeno, Structural and magnetic aspects of the metal-insulator transition in Ca<sub>2-x</sub>Sr<sub>x</sub>RuO<sub>4</sub>, *Phys. Rev. B* **63**, 174432 (2001).
- [12] P. Steffens, O. Friedt, P. Alireza, W. G. Marshall, W. Schmidt, F. Nakamura, S. Nakatsuji, Y. Maeno, R. Lengsdorf, M. M. Abd-Elmeguid, and M. Braden, High-pressure diffraction studies on Ca<sub>2</sub>RuO<sub>4</sub>, *Phys. Rev. B* **72**, 094104 (2005).
- [13] Z. Fang and K. Terakura, Magnetic phase diagram of Ca<sub>2</sub>RuO<sub>4</sub> governed by structural distortions, *Phys. Rev. B* **64**, 020509(R) (2001).
- [14] G. Zhang and E. Pavarini, Mott transition, spin-orbit effects, and magnetism in Ca<sub>2</sub>RuO<sub>4</sub>, *Phys. Rev. B* **95**, 075145 (2017).
- [15] S. Kunkemöller, D. Khomskii, P. Steffens, A. Piovano, A. A. Nugroho, and M. Braden, Highly Anisotropic Magnon Dispersion in Ca<sub>2</sub>RuO<sub>4</sub>: Evidence for Strong Spin Orbit Coupling, *Phys. Rev. Lett.* **115**, 247201 (2015).
- [16] F. Nakamura, T. Goko, M. Ito, T. Fujita, S. Nakatsuji, H. Fukazawa, Y. Maeno, P. Alireza, D. Forsythe, and S. R. Julian, From Mott insulator to ferromagnetic metal: A pressure study of Ca<sub>2</sub>RuO<sub>4</sub>, *Phys. Rev. B* **65**, 220402 (2002).
- [17] S. Nakatsuji and Y. Maeno, Quasi-Two-Dimensional Mott Transition System Ca<sub>2</sub>RuO<sub>4</sub>, *Phys. Rev. Lett.* **84**, 2666 (2000).
- [18] F. Nakamura, M. Sakaki, Y. Yamanaka, S. Tamaru, T. Suzuki, and Y. Maeno, Electric-field-induced metal maintained by current of the Mott insulator Ca<sub>2</sub>RuO<sub>4</sub>, *Sci. Rep.* **3**, 2536 (2013).
- [19] S. Whitehead, *Dielectric Breakdown of Solids* (Oxford University Press, Oxford, 1953).
- [20] Y. Taguchi, T. Matsumoto, and Y. Tokura, Dielectric breakdown of one-dimensional Mott insulators Sr<sub>2</sub>CuO<sub>3</sub> and SrCuO<sub>2</sub>, *Phys. Rev. B* **62**, 7015 (2000).
- [21] C. Sow, S. Yonezawa, S. Kitamura, T. Oka, K. Kuroki, F. Nakamura, and Y. Maeno, Current-induced strong diamagnetism in the Mott insulator Ca<sub>2</sub>RuO<sub>4</sub>, *Science* **358**, 1084 (2017).
- [22] H. Zhao, B. Hu, F. Ye, C. Hoffmann, I. Kimchi, and G. Cao, Nonequilibrium orbital transitions via applied electrical current in calcium ruthenates, *Phys. Rev. B* **100**, 241104 (2019).
- [23] R. Okazaki, Y. Nishina, Y. Yasui, F. Nakamura, T. Suzuki, and I. Terasaki, Current-induced gap suppression in the Mott insulator Ca<sub>2</sub>RuO<sub>4</sub>, *J. Phys. Soc. Jpn.* **82**, 103702 (2013).
- [24] J. Zhang, A. S. McLeod, Q. Han, X. Chen, H. A. Bechtel, Z. Yao, S. N. Gilbert Corder, T. Ciavatti, T. H. Tao, M. Aronson, G. L. Carr, M. C. Martin, C. Sow, S. Yonezawa, F. Nakamura, I. Terasaki, D. N. Basov, A. J. Millis, Y. Maeno, and M. Liu, Nano-Resolved Current-Induced Insulator-Metal Transition in the Mott Insulator Ca<sub>2</sub>RuO<sub>4</sub>, *Phys. Rev. X* **9**, 011032 (2019).
- [25] G. Mattoni, S. Yonezawa, and Y. Maeno, Diamagnetic-like response from localized heating of a paramagnetic material, *Appl. Phys. Lett.* **116**, 172405 (2020).
- [26] O. Friedt, P. Steffens, M. Braden, Y. Sidis, S. Nakatsuji, and Y. Maeno, Strongly Enhanced Magnetic Fluctuations in a Large-Mass Layered Ruthenate, *Phys. Rev. Lett.* **93**, 147404 (2004).
- [27] P. Steffens, O. Friedt, Y. Sidis, P. Link, J. Kulda, K. Schmalzl, S. Nakatsuji, and M. Braden, Magnetic excitations in the metallic single-layer ruthenates Ca<sub>2-x</sub>Sr<sub>x</sub>RuO<sub>4</sub> studied by inelastic neutron scattering, *Phys. Rev. B* **83**, 054429 (2011).
- [28] J. Bertinshaw, N. Gurung, P. Jorba, H. Liu, M. Schmid, D. T. Mantadakis, M. Daghofer, M. Krautloher, A. Jain, G. H. Ryu, O. Fabelo, P. Hansmann, G. Khaliullin, C. Pfleiderer, B. Keimer, and B. J. Kim, Unique Crystal Structure of Ca<sub>2</sub>RuO<sub>4</sub> in the Current Stabilized Semimetallic State, *Phys. Rev. Lett.* **123**, 137204 (2019).
- [29] S. Kunkemöller, E. Komleva, S. V. Streltsov, S. Hoffmann, D. I. Khomskii, P. Steffens, Y. Sidis, K. Schmalzl, and M. Braden, Magnon dispersion in Ca<sub>2</sub>Ru<sub>1-x</sub>Ti<sub>x</sub>O<sub>4</sub>: Impact of spin-orbit coupling and oxygen moments, *Phys. Rev. B* **95**, 214408 (2017).
- [30] C. Cirillo, V. Granata, G. Avallone, R. Fittipaldi, C. Attanasio, A. Avella, and A. Vecchione, Emergence of a metallic metastable phase induced by electrical current in Ca<sub>2</sub>RuO<sub>4</sub>, *Phys. Rev. B* **100**, 235142 (2019).
- [31] A. Mansingh, R. Singh, and S. Krupanidhi, Electrical switching in single crystal VO<sub>2</sub>, *Solid-State Electron.* **23**, 649 (1980).
- [32] A. F. Volkov and S. M. Kogan, Physical phenomena in semiconductors with negative differential conductivity, *Sov. Phys. Usp.* **11**, 881 (1969).
- [33] S. Kumar, M. D. Pickett, J. P. Strachan, G. Gibson, Y. Nishi, and R. S. Williams, Local temperature redistribution and structural

- transition during joule-heating-driven conductance switching in VO<sub>2</sub>, *Adv. Mater.* **25**, 6128 (2013).
- [34] C. N. Berglund, Thermal filaments in vanadium dioxide, *IEEE Trans. Electron Devices* **16**, 432 (1969).
- [35] S. Zhang, M. A. Kats, Y. Cui, Y. Zhou, Y. Yao, S. Ramanathan, and F. Capasso, Current-modulated optical properties of vanadium dioxide thin films in the phase transition region, *Appl. Phys. Lett.* **105**, 211104 (2014).
- [36] S. Stille, C. Lenser, R. Dittmann, A. Koehl, I. Krug, R. Muenstermann, J. Perlich, C. M. Schneider, U. Klemradt, and R. Waser, Detection of filament formation in forming-free resistive switching SrTiO<sub>3</sub> devices with ti top electrodes, *Appl. Phys. Lett.* **100**, 223503 (2012).
- [37] The specific heat at room temperature is taken from Ref. [48] for 8.5% Mn-doped Ca<sub>2</sub>RuO<sub>4</sub>. The temperature increase rate is calculated with  $\Delta T = \frac{p}{C_p n_V}$ , where  $p$  is the power density in W cm<sup>-3</sup>,  $C_p$  the specific heat in Jmol<sup>-1</sup> K<sup>-1</sup>, and  $n_V$  the amount of substance in molcm<sup>-3</sup>.
- [38] The values of atomic distance between the Ru site and the basal oxygen sites Ru-O(1)(avg.) reported in Ref. [28] for the S\* phase at 130 K (in Refs. [10,11] for the S phase at 240 K) amount to 2.003(2.004) Å. The Ru-O(2) distance amounts in both cases to 1.979 Å, which yields an averaged Ru-O distance of 1.995(1.996) Å. The rotation angle  $\Phi$  of the RuO<sub>6</sub> octahedra around the  $c$  axis amounts to 11.874(11.91) degrees. The basal plane is tilted in respect to the  $ab$  plane by  $\Theta$ -O(1) 12.43(12.23) degrees and the tilt angle  $\Theta$ -O(2) between the Ru-O(2) bond and the  $c$  axis amounts to 10.65(10.2) degrees.
- [39] A. Khachaturian, *Theory of Structural Transformations in Solids* (Wiley, New York, 1983).
- [40] A. G. Khachatryan, S. M. Shapiro, and S. Semenovskaya, Adaptive phase formation in martensitic transformation, *Phys. Rev. B* **43**, 10832 (1991).
- [41] S. Bartsch and U. Oelfke, Line focus x-ray tubes a new concept to produce high brilliance x-rays, *Phys. Med. Biol.* **62**, 8600 (2017).
- [42] O. Breunig, Z. Wang, A. A. Taskin, J. Lux, A. Rosch, and Y. Ando, Gigantic negative magnetoresistance in the bulk of a disordered topological insulator, *Nat. Commun.* **8**, 15545 (2017).
- [43] J. Dec, Praelastic and ferroelastic interfaces, *Phase Transit.* **45**, 35 (1993).
- [44] A. L. Roytburd, Elastic domains and polydomain phases in solids, *Phase Transit.* **45**, 1 (1993).
- [45] J. W. Seo and D. Schryvers, TEM investigation of the microstructure and defects of CuZr martensite. Part I: Morphology and twin systems, *Acta Mater.* **46**, 1165 (1998).
- [46] S. Kaufmann, U. K. Röbber, O. Heczko, M. Wuttig, J. Buschbeck, L. Schultz, and S. Fähler, Adaptive Modulations of Martensites, *Phys. Rev. Lett.* **104**, 145702 (2010).
- [47] D. I. Khomskii and K. I. Kugel, Why stripes? Spontaneous formation of inhomogeneous structures due to elastic interactions, *Europhys. Lett.* **55**, 208 (2001).
- [48] T. F. Qi, O. B. Korneta, S. Parkin, J. Hu, and G. Cao, Magnetic and orbital orders coupled to negative thermal expansion in Mott insulators Ca<sub>2</sub>Ru<sub>1-x</sub>M<sub>x</sub>O<sub>4</sub> (M = Mn and Fe), *Phys. Rev. B* **85**, 165143 (2012).